2022 IEEE/RSJ International Conference on Intelligent Robots and Systems (IROS)
October 23-27, 2022, Kyoto, Japan

Manual Maneuverability: Metrics for Analysing and Benchmarking Kinesthetic Robot Guidance

Robin Jeanne Kirschner[1], Florian Martineau, Nico Mansfeld, Saeed Abdolshah and Sami Haddadin

***Abstract*— Kinesthetic teaching of collaborative robots is applied for intuitive and flexible robot programming by demonstration. This enables non-experts to program such robots on the task-level. Multiple strategies exist to teach velocity- or torque-controlled robots and, thus, the maneuverability among commercial robots differs significantly. However, currently there exists no metric that quantifies how "well" the robot can be guided, e.g., how much effort is required to initiate a motion. In this paper, we propose standardized procedures to quantitatively assess robot manual maneuverability. First, we identify different motion phases during kinesthetic teaching. For each phase, we then propose metrics and experimental setups to evaluate them. The experimental protocols are applied to the proprietary teaching schemes of five commercial robots, namely the KUKA LWR iiwa 14, Yuanda Yu+, Franka Emika robot, and Universal Robot's UR5e and UR10e. The experimental comparison highlights distinct differences between the robots and shows that the proposed methods are a meaningful contribution to the performance and ergonomics assessment of collaborative robots.**

I. INTRODUCTION

Robot motion performance metrics are important criteria to evaluate whether a manipulator is suitable for certain tasks. Many performance criteria have been established and standardized, e.g., path accuracy and pose repeatability [1]. With modern collaborative robots, task programming has become simple and intuitive, as such systems offer kinesthetic guidance functionalities [2], [3], [4]. Kinesthetic guidance allows the robot user to manually maneuver the robot to a desired pose in the workspace or kinematically reconfigure the robot. This feature is often used for programming by demonstration [5], [6], where either the end-effector pose or the entire path is recorded [7], [5]. Kinesthetic teaching allows improving flexibility in production lines with small batches that require time-efficient (re-)programming [6], [3]. It can be realized with different control strategies [8], [9], [10], [11]. A comparison of these strategies showed that they affect user acceptance [7], [2] as well as task-dependent parameters the length of a trajectory [5]. While user studies highlight the practical benefits of kinesthetic guidance [5] and the importance of proper design of this functionality [2], [7], no quantitative metrics for assessing kinesthetic guidance have been proposed until now (to the best of the authors' knowledge). A benchmark for kinesthetic robot guidance can aid the development of kinesthetic guidance implementations by providing a generalized evaluation procedure for robot comparison. In our previous work [12], we introduced an initial metric for kinesthetic guidance which we referred to as *manual maneuverability*. This metric describes the force required to guide a robot at the end-effector along a one-dimensional line in the task space. It was evaluated for a Universal robot's UR5e, UR10e, and Franka Emika robot in the y-direction for a constant motion speed of $0.25\,\mathrm{m/s}$.

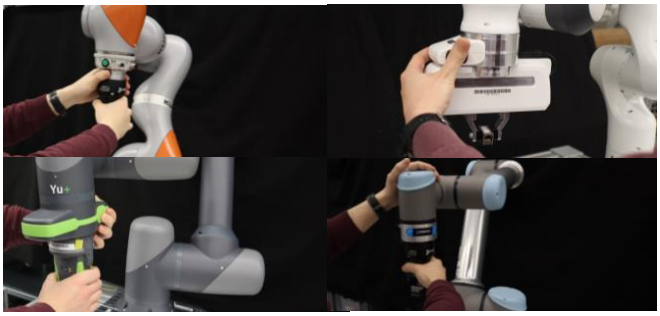

Fig. 1. Kinesthetic guidance of a Yuanda Yu+, Franka Emika, KUKA LWR iiwa 14, and UR10e robot for programming by demonstration.

In this work, we aim for a deeper comprehension of manual maneuverability. From our practical experience with different collaborative robots, we first identify different motion phases during kinesthetic teaching and parameters that users typically consider important, e.g., the force required to guide the robot. For each phase, we then propose metrics that evaluate the ease of robot kinesthetic guiding. For this, we propose further metrics for manual maneuverability to include information on the quality of motion steadiness defined as the deviation from a desired path in Cartesian space, information on the quality of the robot joint friction compensation, and the overall required energy for an understanding of the ergonomic properties of the guiding. For the proposed set of metrics, we observe the influence of robot factors and provide an overview of the metrics results for five different commercially available collaborative robots. The systems represent typical cobots on the market with varying built-in kinesthetic guiding controllers namely the Kuka LWR iiwa 14 (LWR), Franka Emika robot (FE), Yuanda's Yu+, Universal Robot's UR5e, and UR10e.

This paper is structured as follows. In Sec. II, we summarize the state of the art of kinesthetic robot guidance and motion performance metrics. In Sec. III, the kinesthetic guidance phases are identified and described. In Sec. IV, we propose the manual maneuverability metrics as well as experimental protocols to evaluate them. Sec. V presents the results for the considered robots. Sec. VI discusses the metrics, and Sec. VII concludes the paper.

All authors are with Institute for Robotics and Systems Intelligence, Munich Institute of Robotics and Machine Intelligence (MIRMI), Centre for Tactile Internet with Human-in-the-Loop (CeTI), Technical University of Munich, 80992 Munich, Germany robin-jeanne.kirschner@tum.de

2022 IEEE/RSJ International Conference on Intelligent Robots and Systems (IROS) | 978-1-6654-7927-1/22/$31.00 ©2022 IEEE | DOI: 10.1109/IROS47612.2022.9981864

TABLE I

MANUAL MANEUVERABILITY METRICS

Motion phase	A	B		C		all
Metrics	Minimum motion force (MF)	Motion steadiness mean and maximum (MS, MS_{max})		N-dimensional guiding force and deviation (GF_N, GD_N)		N-dimensional guiding energy (E_N)
Definition	Force required to overcome static friction	Mean deviation in x- and z-direction from the expected guiding path.	Maximum deviation in x- and z-direction from the external force direction.	External force during guidance along an N-dimensional path.	External force standard deviation during guidance along an N-dimensional path.	Interaction energy for guidance along a N-dimensional path.
Test setup	3D-gantry with $d = 10\,\mathrm{mm}$, $v = 2\,\mathrm{mm/s}$, and $a = 1\,\mathrm{mm/s^2}$	Path tracking via Faro X Laser Tracker for constant acceleration by weights and pulley, cf. Fig. 5		3D gantry with $d \geq 400\,\mathrm{mm}$, $v = 50$–$250\,\mathrm{mm/s}$, and $a = 1000\,\mathrm{mm/s^2}$		
Equation	(1)	(3)	(4)	(5)	(6)	(7)
Observed factors	x-, y-, z-direction, Center/front point, Five robot types	Center/front point, Line/Free guide, Five robot types		Center/front point, Line/Free guide, Stiff/default/compliant behavior, Five robot types		Center/front point, Line/Free guide, Five robot types

II. STATE OF THE ART

First, we give a brief overview of methods for enabling kinesthetic robot motion, followed by a brief overview of metrics for robot motion performance. A mechanical solution is to compensate gravitation for manually guiding a robot, actuated or under-actuated counterweights are used, e.g., by adding auxiliary counterweights to the robot link [13], appropriate distribution of motor weight [14], or simple mechanical structures for hand-operated balanced manipulators, e.g., spring mechanisms that can be mounted directly or that are attached via cable and pulley [15], [16], [17]. Alternatively, kinesthetic guidance can be realized by compensating for the robot gravity torque, admittance control [10], [11], or impedance control, where translational or rotational stiffness is set to zero, for example [8] [18]. In this context, it shall be noted that torque-control based on joint torque sensing as in [19] usually has better performance than position-based methods, which require external sensors or torque estimation via motor current or position measurement [20], [21]. To produce more precise motions for manual programming by demonstration, machine learning methods can be applied to correct imperfect trajectories [22] or to provide refinement pipes around desired trajectories to limit deviation from a desired path while guiding the robot [23], [9].

Recently, several task-based performance comparisons as well as metrics for robot performance have been proposed, and some of these metrics have found their way into standards. For example, the standardized measurements for evaluating a robot's motion performance include pose repeatability and path accuracy, which are defined by DIN EN ISO 9283:1998 [1]. Furthermore, task-dependent motion performance benchmarks are proposed using efficiency metrics such as planning time, success rate, time-bound success rate, and motion performance described by the length of the computed plan [24]. In our previous work, we introduced manual maneuverability as the force required to guide robotic end-effectors [12]. In this work, we aim for a deeper comprehension of manual maneuverability.

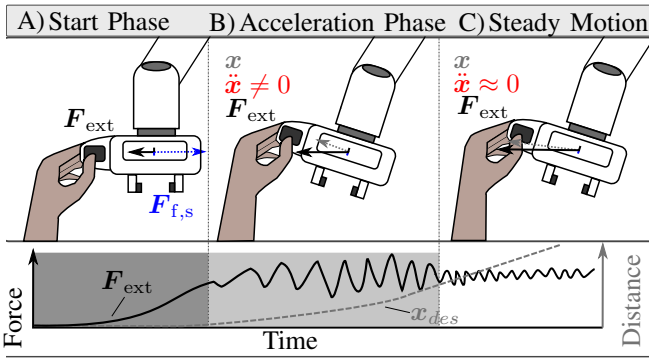

Fig. 2. Qualitative representation of phases during the kinesthetic guidance that can be experienced by the robot user and the force curve $\boldsymbol{F}_{\mathrm{ext}}$ required to guide the robot along a predefined trajectory $\boldsymbol{x}_{des}$. All phases contribute to the manual maneuverability.

III. KINESTHETIC GUIDANCE ANALYSIS

In this section, we describe three motion phases that typically occur during kinesthetic teaching based on personal experience. We call the three phases *start*, *acceleration*, and *steady motion* that are depicted in Fig. 2.

Start phase When the user exerts an external guiding force at the robot, this force needs to overcome the static friction so that at least one joint moves; see Fig. 2 A). As long as the external force $\boldsymbol{F}_{\mathrm{ext}}$ is below the static frictional force $\boldsymbol{F}_{\mathrm{f,s}}$, the robot is at rest.

Acceleration phase After the motion has been initiated, the user expects the robot to move in the direction of the applied force. However, robots often deviate from the desired direction and the force required to move the system typically oscillates significantly; see Fig. 2 B). This is can be explained by the sequential overcoming of the static friction force in the joints.

Steady motion phase As soon as the motion of all involved joints has been initiated and the acceleration phase is completed ($\ddot{x} \approx 0$), the robot can typically be guided smoothly, i.e., less oscillations occur; see Fig. 2 C). In this phase, the robot's manual maneuverability, i.e.,

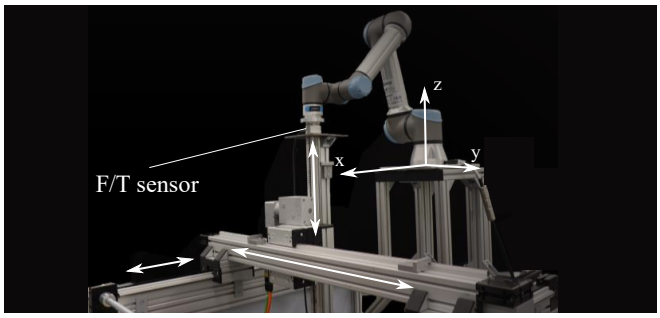

Fig. 3. Setup for automated analysis of the robot guiding force using a 3D gantry structure, with linear units and a force-torque (F/T) sensor.

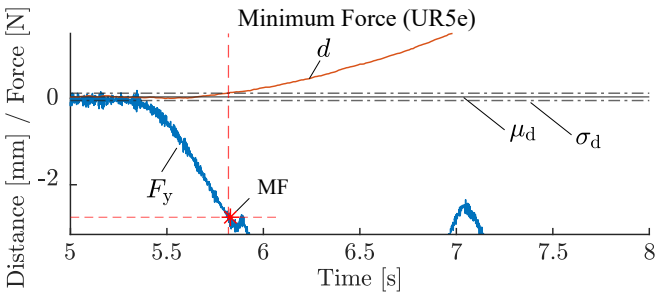

Fig. 4. Force and displacement profile to evaluate the force required to overcome static friction when trying to move a robot end-effector. Exemplary depicted is the values for a UR5e robot which is moved in y-direction from its central reference cube location at $v = 2\,\mathrm{mm/s}$ and with an acceleration of $a = 1\,\mathrm{mm/s^2}$.

the effort required to guide the robot, depends on the dynamic friction, the robot's (coupled) inertial properties and configuration as well as the control algorithm.

In the following, we define and elaborate metrics for each motion phase and propose experimental protocols to evaluate them. The metrics are summarized in Tab. I and ordered by motion phase.

IV. METRIC DEFINITION

For all metrics, we apply the robot reference cubes defined by DIN EN ISO 9283:1998 [1] as a spacial reference system. We refer to the center of the reference cube as C2 and name the other points according to the points of the compass with the layers 1-3 corresponding to lower, middle, and upper layer, e.g., NW1 is the lower corner position of the cube farthest from the robot base.

A. Minimum motion force

The static friction of the robot joints requires an initial breakout force to move the robot. The *minimum motion force (MF)* metric attempts to answer the question how high this force is. Typically, this breakout force is described by force and displacement over time. To measure MF, the robot end-effector, which is in kinesthetic guidance mode, is displaced while the force acting on the end-effector is continuously measured. For this purpose, we use a extended version of the experimental setup in [12], as shown in Fig. 3. The setup consists of a gantry and a K6D40 force-torque sensor from ME Messysteme integrated via a compactRio system from National Instruments with a total force measurement accuracy $A_{\mathrm{F,gantry}} = 0.17 \pm 0.0071N$. The robot flange is connected to the sensor and the kinesthetic guidance is activated. Then, the gantry moves the robot flange from one defined point to another along a defined path with a constant acceleration profile $a = 1\,\mathrm{mm/s^2}$.

We start the force and displacement measurement simultaneously and obtain force and displacement profiles as shown in Fig. 4. To measure whether a displacement has occurred, we obtain the mean μ_d and standard deviation σ_d of the position measurement while the linear motors are not in motion. At the time where the displacement is $d(t) > \mu_\mathrm{d} + \sigma_\mathrm{d}$, we define the beginning of the motion. MF is then expressed as

$$\mathrm{MF} = |F(t_f)|, \quad d(t_f) > \mu_\mathrm{d} + \sigma_\mathrm{d}\,. \tag{1}$$

In Fig. 4 we provide an example where $\mathrm{MF} = 2.75\,\mathrm{N}$.

B. Motion steadiness

After the static friction is overcome, the robot end-effector accelerates. In this motion phase, there is often a high deviation of the external guiding forces, as shown in Fig. 2, which is caused partly by a discrepancy between the applied force direction and the resulting direction of motion of the robot, which we refer to as *motion steadiness (MS)*. MS is defined as the deviation of the measured robot path from the desired one. Different robot kinesthetic guidance modes can lead to different results for the MS, as depicted in Fig. 5 for 6-dimensional (Free) and one-dimensional guidance mode (Line).

To measure MS, we propose the setup shown in Fig. 6. It consists of a horizontally aligned steel cable connected to the robot flange with a weight attached on the other side. Thus, a one-dimensional horizontal force acts on the robot end-effector. A Faro X laser tracker with a spherical retroreflector attached to the robot flange is used to measure the Cartesian position of the robot end-effector. The additional weight to the robot flange of the retroflector and adapter plates of $633\,\mathrm{g}$ and the displacement of the center of mass in the z-direction of $75\,\mathrm{mm}$ are set as the additional robot tool parameters.

The motion of the robot in the y-direction is initiated by the lowest weight required to move the end-effector, which is determined experimentally. For the FE, it is $0.2\,\mathrm{kg}$ with free guidance and $0.4\,\mathrm{kg}$ with constrained guidance. The ideal robot end-effector trajectory is assumed to be a line along the y-axis. The position deviation vector between the measured x-position $\boldsymbol{x}$ and the ideal x-position $\boldsymbol{x}_\mathrm{ideal}$ as well as the measured $\boldsymbol{z}$ and the ideal z-position $\boldsymbol{z}_\mathrm{ideal}$ described by

$$\boldsymbol{p}_\mathrm{diff} = [\boldsymbol{x} - \boldsymbol{x}_\mathrm{ideal}; \boldsymbol{z} - \boldsymbol{z}_\mathrm{ideal}]\,, \tag{2}$$

is then used to define the average deviation as

$$\mathrm{MS} = \mu_{p,\mathrm{diff}} = \frac{1}{m}\sum_{i=1}^{m} |\boldsymbol{p}_{\mathrm{diff},i}|\,. \tag{3}$$

The maximum deviation in x- and z-direction is given by

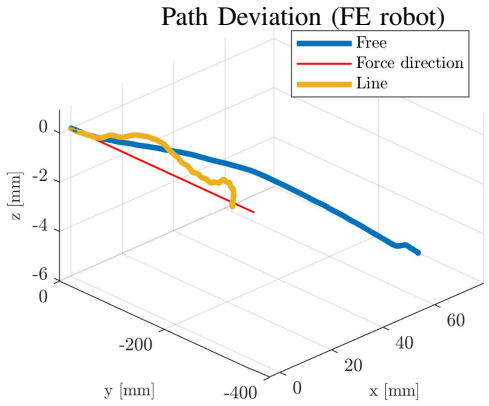

Fig. 5. Exemplary deviation of the robot motion at constant acceleration observed for the FE. Depicted in blue the robot controller enables unrestricted robot motion while the yellow trajectory uses a Cartesian motion constraint in y-direction. Notable is the deviation between the red direction of applied force and the two resulting motions.

$$\mathrm{MS}_{\max} = \max\left(\boldsymbol{p}_{\mathrm{diff}}\right) . \tag{4}$$

The most interesting aspect of MS that we observe is that it depends on the influence of the different guidance modes and whether they are affected by the robot stiffness. Therefore, we use the FE to test different guidance modes with different compliance settings. The compliance settings refer to the settings in the Desk interface for the FE by defining $0\,\%$ compliance for all joints and in Cartesian space for the stiff setting, $100\,\%$ compliance for the compliant setting, and the default settings. The following joint configurations q_{C} and q_{N} are used for the starting configuration of the FE:

q_{C} = [-0.01, -0.14, 0.01, -2.35, -0.01, 2.20, -0.00] rad,
q_{N} = [-0.01, 0.45, 0.01, -1.57, -0.01, 2.02, -0.01] rad.

C. Guiding force and deviation

The *guiding force metric* ($\mathrm{GF_N}$) quantifies the force required to guide the robot end-effector with a defined velocity profile along a path in R^{N}. The strongly related guidance deviation ($\mathrm{GD_N}$) explains whether this force is constant or whether there is a strong force oscillation [12]. Subscript N refers to the number of DoF considered for the executed motion. We denote the guiding force of a one-dimensional motion by $\mathrm{GF_1}$, a two-dimensional motion by $\mathrm{GF_2}$, and a three-dimensional motion by $\mathrm{GF_3}$, where the N-dimensional motion, refers to the paths depicted by Fig. 7.

To measure these two metrics, we previously proposed a one-dimensional test bed that measures the force required to move a robot along the y-direction of the robot's base frame [12]. Now, we used the extended test rig to include 2- and 3-dimensional motion, which are motivated as follows:

1D The 1D line between two positions is the most basic motion in Cartesian space.

2D When guiding the robot from one position to another, we observe that most users pull the robot towards themselves to some extent, which results in a curved trajectory.

3D During the implementation of a task or in case of an error, the robot may stop anywhere in the workspace. In that case, one wants to bring the robot back to a default position, in our case the center of the ISO cube. In the 3D case, we consider a linear path from the robot workspace boundary to ISO cube center; cf. Fig. 7.

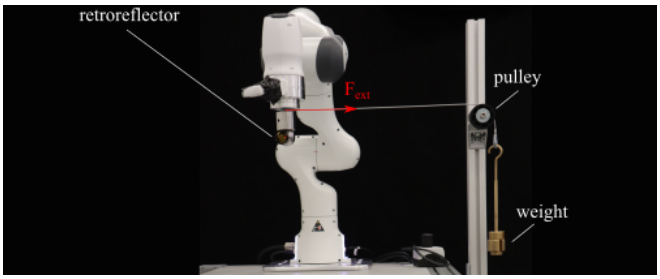

Fig. 6. Experimental setup to define the motion steadiness of the robot end-effector when a constant force is applied. A Faro laser tracker is used to track the end-effector position. A steel rope with additional mass is attached to the end-effector and horizontally aligned with a pulley.

$\mathrm{GF_N}$ is defined as the average force required to guide the robot with constant velocity along a N-dimensional trajectory

$$\mathrm{GF_N} = \mu_{\mathrm{F}} = \frac{1}{m}\sum_{i=1}^{m} |f_i| , \tag{5}$$

where f_i denotes its force at each measurement i and m is the total size of the data set.

Additionally, the guiding deviation $\mathrm{GD_N}$ is given as

$$\mathrm{GD_N} = \sigma_{\mathrm{F}} = \sqrt{\frac{1}{m}\sum_{i=1}^{m} \left(|f_i| - \mu_{\mathrm{F}}\right)^2} . \tag{6}$$

A typical force-time profile is depicted in Fig. 8. For evaluation, we consider the phase of constant velocity for the forward motion as shown in the upper graph of Fig. 8.

D. Kinesthetic guidance energy

To include the robot kinesthetic guidance to ergonomic evaluations, e.g., the average guidance energy can be used [25], [26]. Therefore, we define an energy-based metric for all three phases of kinesthetic guidance, called *N-dimensional kinesthetic guidance energy* ($\mathrm{E_N}$). It is defined as

$$\mathrm{E_N} = \int_0^d f_{\mathrm{i}}(x)\, dx , \tag{7}$$

where x is the current travelled distance and d is the total distance. The measurement follows the same experimental procedure as $\mathrm{GF_N}$. In contrast to $\mathrm{GF_N}$, $\mathrm{E_N}$ is calculated along the entire guided path.

For our analysis we consider the robots' proprietary kinesthetic guidance methods, which may allow different guiding modes in Cartesian space for the robot end-effector, referred to as Line (1D), Plane (2D), Crane (3D), and Free (6D).

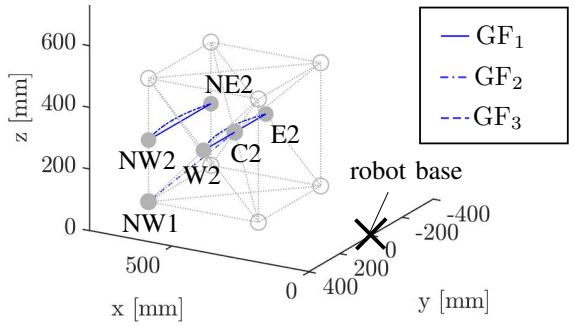

Fig. 7. Robot reference cube and considered guiding paths for the N-dimensional guiding force metric.

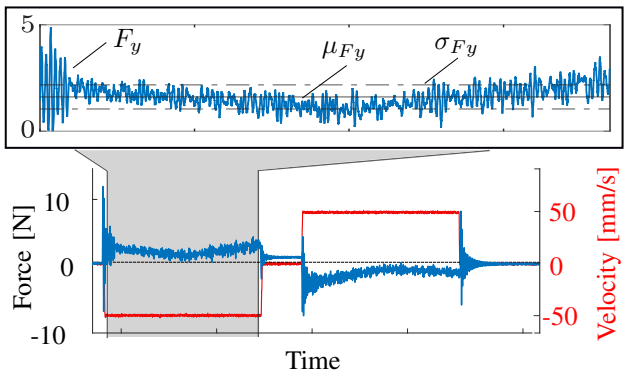

Fig. 8. Example for the guiding force profile FE at 50 mm/s. The forward and backward motion along the trajectory are recorded. The forward motion without acceleration phases is used to determine the guiding force.

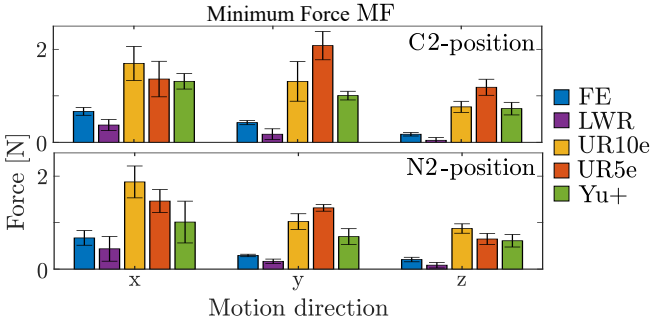

Fig. 9. Results for the MF of FE, LWR, UR10e, UR5e, and Yu+ for motions in x-, y-, and z-direction of the robot base frame and in C2- and N2-position of the respective robot reference cube.

E. Evaluation

In the following, we demonstrate the proposed manual maneuverability metrics considering the different influencing factors:

a) robot *configuration* described by the end-effector location (p) in the robot reference cube,
b) the *dimension* and *direction* of the motion,
c) built-in *guidance mode*,
d) guiding *velocities*, and
e) the robot joint and Cartesian *compliance*.

For each metric, the most relevant parameters are selected. All metrics are evaluated using respectively 10 or 30 experimental trials. To validate whether the metrics are suitable for evaluating different types of robots, the assumption of normal distribution of each set of results is first validated by a Kolmogorov-Smirnoff test. We conduct a one-way analysis of variance (ANOVA) at the $\alpha = 0.05$ significance level to validate the existence of significant difference between the groups of robot types. Finally, the significance of the metric means between all robots are evaluated using a Tukey-Kramer multiple comparison test (also referred to as post-hoc test). All tests are conducted using the MATLAB Statistics and Machine Learning Toolbox (R2022a); the results are listed in Table III.

V. RESULTS

In this section, we describe the results of the manual maneuverability metrics.

A. Minimum motion force

The results for MF are depicted in Fig. 9 as mean and standard deviation over $n = 10$ experiments. We observe that all robots' breakout force is less than $\approx$2 N or less. The LWR requires the least breakout force (0.1–0.5 N) followed by the FE robot (0.2–0.7 N). The UR10e, UR5e, and Yu+ show higher breakout forces in general between 0.7 N and 2.0 N. All robots require the least MF when moved in z-direction.

B. Motion steadiness

Fig. 10 shows the results for MS and $\mathrm{MS}_{\max}$ as an average over $n = 10$ trials for the FE using different robot compliance settings, Line or Free guidance mode, and starting point C2 and N2. We find that the Line guidance mode allows motion along the force direction and only deviates by a maximum of 9.9 mm at the FE's default compliance setting and N2 as the starting point. The average deviation of the Line mode never exceeds MS = 1.5 mm. For the Free guidance mode, on the other hand, an average deviation of up to MS = 48.2 mm and a maximum deviation of $\mathrm{MS}_{\max} = 108.3$ mm were measured for stiff robot compliance and starting point N2. Except for the Free guidance from N2, none of the experimental results support the theory that the robot compliance setting can affect the motion steadiness. The results vary slightly between the starting points N2 and the C2 for the Free guidance mode. For Line, they are negligible. Fig. 11 compares all five robot types using their available guidance modes. For FE and UR5e with URSoftware version 5.11.6, a Line mode is applied while the other robots offer Free mode. Due to a high deviation which caused the laser tracker to fail tracking the retroreflector, no results for the UR10e and LWR can be provided. A significant difference between the three robots can only be observed based on the guiding modes which differ between Yu+ (Free) and UR5e and FE (Line).

C. Guiding force and deviation

The results for $\mathrm{GF_N}$ with (5) and $\mathrm{GD_N}$ with (6) are presented using the mean and standard deviation over n = 30 trials. First, we analyse the influence of guidance velocity on $\mathrm{GF_N}$ and $\mathrm{GD_N}$ with $n = 10$ experimental trials per velocity and dimension, shown in Fig. 12 for the path $\overline{W2E2}$. We observe no significant effect of velocity on $\mathrm{GF_N}$ or $\mathrm{GD_N}$

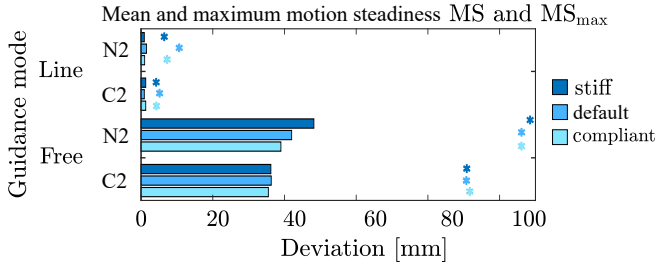

Fig. 10. Influence of the guidance mode, start position, and robot compliance settings for the FE on the average motion steadiness MS and the maximum deviation from the desired path $\mathrm{MS}_{\max}$.

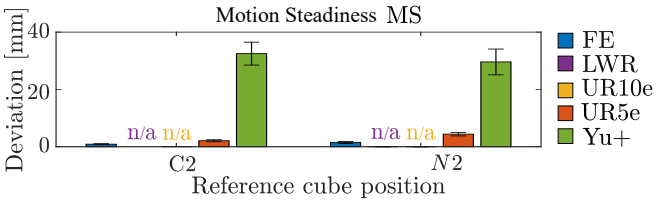

Fig. 11. Motion steadiness results for FE, UR5e, and Yu+.

for any of the dimensions. Consequently, we perform the following measurements with $v = 250\,\mathrm{mm/s}$, since it is the maximum permissible velocity for kinesthetic guidance [4].

Next, we investigate whether it is important to take measurements inside the robot reference cube by considering the curved paths between $W2$ and $E2$ and between $NW2$ and $NE2$, where the latter one moves outside the cube. The mean results in Table II for $n = 10$ trials show a significant increase in GF_2 outside the reference cube. Also GD_2 slightly increases outside the reference cube. The increasing forces are most likely a result of the robot configurations moving towards a singularity.

We consider the influence of the number of motion dimensions on GF_N and GD_N for the FE in the Free and constrained guidance modes of Line, Plane, and Crane, respectively, as shown in Fig. 13. GF_N increases with the number of dimensions, while GD_N remains comparable. This results partly from the rigid attachment of the robot flange to the sensor. For a one-dimensional motion, the resulting constraint forces can be sufficiently eliminated since only the force in the direction of motion is considered. However,

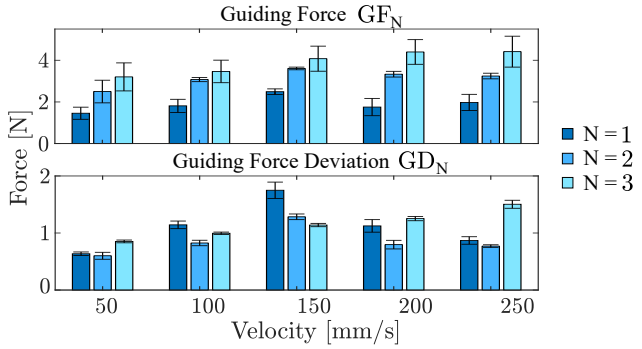

Fig. 12. Influence of the guiding velocity on GD_N and GF_N for the FE at C-position and one-dimensional motion in y-direction, circular two-dimensional motion, and three-dimensional motion from C2 to NW1 of the robot reference cube. Each mean is built from $n = 10$ trials.

TABLE II

RESULTS FOR GF_2 AND GD_2 INSIDE AND OUTSIDE THE ROBOT REFERENCE CUBE

	$W2$ to $E2$		$NW2$ to $NE2$	
Robot	GF_2 [N]	GD_2 [N]	GF_2 [N]	GD_2 [N]
FE Plane	3.2 ± 0.05	0.8 ± 0.03	6.0 ± 0.14	1.3 ± 0.06
FE Free	1.7 ± 0.14	0.6 ± 0.02	5.3 ± 0.15	1.06 ± 0.6

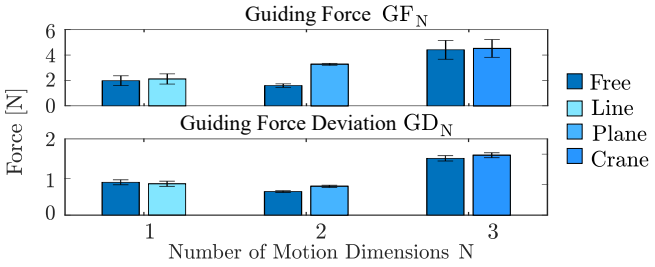

Fig. 13. Influence of the number of dimensions of the motion on GD_N and GF_N for the FE in Free mode, in Line, Plane, and Crane mode respectively at the central motion path. Each mean is built from $n = 10$ trials.

as the number of dimensions increases, additional constraint forces are also measured. We therefore propose to benchmark kinesthetic robot guidance for one-dimensional trajectories using our test bed.

Finally, we provide the results of a benchmark for the kinesthetic guidance force of the five robots LWR, Yu+, UR5e, UR10e, and FE for a one-dimensional trajectory in the y-direction from $W2$ to $E2$ and from $NW2$ to $NE2$. For all robots, we observe slightly lower GF_1 in the distal position to the robot base coordinates compared to the central trajectory of the robot reference cube, which is likely due to the mass distribution of the robot. Overall, we observe significant differences between the different systems and their built-in free kinesthetic guidance modes. For the LWR, we used the built-in impedance controller for kinesthetic guidance as it showed the best performance. Please note that there are also different options for activating kinesthetic guidance for this robot.

D. Kinesthetic Guiding Energy

For the last metric, we estimate the required workload to perform kinesthetic guidance with any of the five robots along the one-dimensional path. The measurements are based on GF_N and the results are depicted by Fig. 15. The guidance interaction energy differs slightly from GF_N as for robots with greater mass, like the LWR the influence of the acceleration phase is higher than for light robots like the FE. The difference between all robots measurements is significant with p besides the ones for LWR and FE in $\overline{W2E2}$ and for LWR and Yu+ in $\overline{NW2NE2}$.

E. Statistics

All p-values of the statistical analysis of the metric for different robot types are listed in Table III where all statistically significant results with $p < 5\,\%$ at the respective position are marked green. In most cases statistically significant differences between the robot types are reported. The results

TABLE III

P-VALUES IN % FOR ONE-WAY ANOVA FOR METRICS DIFFERENCE BETWEEN THE ROBOT TYPES.

Robots	MS	MF_x	central / distal MF_y	MF_z	GF_1	GD_1	E_1
FE-LWR	n/a	9.44 / 44.52	16.74 / 11.87	0.1 / < 0.01	98.5 / 99.9	85.0 / 8.3	64.7 / 5.3
FE-UR5e	54.07 / 5.7	< 0.01	< 0.01	< 0.01	< 0.01	< 0.01	< 0.01
FE-UR10e	n/a	< 0.01	< 0.01	< 0.01	< 0.01	< 0.01	< 0.01
FE-Yu+	< 0.01	< 0.01 / 11.43	< 0.01	< 0.01	< 0.01	28.1 / 99.7	< 0.01
LWR-UR5e	n/a	< 0.01	< 0.01	< 0.01	< 0.01	< 0.01	< 0.01
LWR-UR10e	n/a	< 0.01	< 0.01	< 0.01	< 0.01	< 0.01	< 0.01
LWR-Yu+	n/a	< 0.01	< 0.01/ 0.12	< 0.01	< 0.01	87.4 / 18.4	< 0.01
UR5e-UR10e	n/a	3.92 / 3.53	< 0.01	< 0.01	< 0.01 / 0.01	< 0.01	< 0.01
UR5e-Yu+	< 0.01	1.27 / < 0.01	5.6 / < 0.01	94.72 / < 0.01	< 0.01	< 0.01	< 0.01
UR10e-Yu+	n/a	99.26 / 1.66	< 0.01	< 0.01	< 0.01	< 0.01	< 0.01

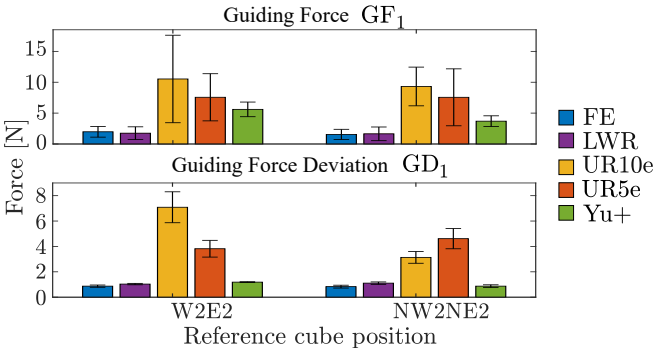

Fig. 14. 1-dimensional guiding force using $n = 30$ trials in y-direction from $W2$ to $E2$ and from $NW2$ to $NE2$ for the Free kinesthetic guidance modes of the FE, LWR, Yu+, UR5e, and UR10e.

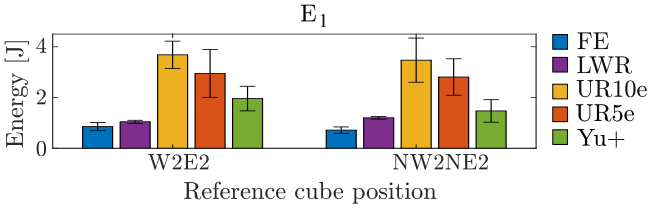

Fig. 15. Interaction energy for the entire guiding procedure in y-direction from $W2$ to $E2$ and from $NW2$ to $NE2$ for the Free kinesthetic guidance modes of the FE, LWR, Yu+, UR5e, and UR10e.

for FE and LWR show few significance, demonstrating an over all similarity in their manual maneuverability performance.

VI. DISCUSSION

Our experiments show that the proposed metrics are well suited to quantify the performance of the proprietary guidance schemes of commercial collaborative robots. We demonstrated that controller type, kinematic configuration, and motion patterns influence manual maneuverability. The minimum required motion force (MF) is in some cases very low and in the range of the sensor resolution of the test bed. To obtain more accurate measurements, high-resolution sensing is required. Nevertheless, our setup allows quantifying the significant difference in the considered robot systems as well as the difference of friction forces depending on the direction of motion. For the motion steadiness (MS) metric, we considered the mean and maximum of the position deviation from the applied force direction. The metrics are especially important for programming entire robot paths via kinesthetic guidance instead of only start and goal poses. The maximum path deviation (MS_{max}) is suited for guiding modes that respect Cartesian constraints, e.g., linear guiding modes. For Free guiding, we observe (as expected) relatively high deviations up to 100 mm. In that case, the MS_{max} metric is less meaningful. For robots that feature only free guiding mode, we therefore omitted the evaluation of this metric. Nevertheless, we measured the average MS for all robots for comparison. The results for GF_N and GD_N showed a dependence on the guiding speeds and robot type. While GF_N is better suited for representing the influence of speed and robot configuration, GD_N is sensitive to robot and controller type. Therefore, both metrics provide valuable insights. Nevertheless, the test procedure showed an influence of the dimension of the motion on the robot guiding force. Thus, we suggest to apply only GF_1 and GD_1 for benchmarking.

VII. CONCLUSIONS

In this paper, we provided a structured analysis of the manual maneuverability of five collaborative and tactile robots. We identified and described three phases of kinesthetic guidance. For each phase, we introduced metrics to quantify the robot manual maneuverability. We evaluated the metrics for five commercial robots. Additionally, we investigated on the influence of different parameters such robot configuration, motion speed, motion direction, stiffness setting, and (proprietary) guidance mode on the manual maneuverability. The comparison based on the proposed metrics demonstrated distinct differences between the tested systems. Overall, we believe that the proposed methods are a meaningful contribution to the performance and ergonomics evaluation of modern robots. They can aid users in selecting a robot for their target application and robot manufacturers in improving the performance and user experience of their systems.

ACKNOWLEDGMENT

The authors would like to thank Sebastian Siegner, Bach Tran, and Felix Spang for their support. We greatly acknowledge the financial support of Vodafone. This work

was supported by Lighthouse Initiative Geriatronics Project Y (LongLeif GaPa gGmbH) and the German Research Foundation (DFG, Deutsche Forschungsgemeinschaft) as part of Germanys Excellence Strategy EXC 2050/1 Project ID 390696704 Cluster of Excellence Centre for Tactile Internet with Human-in-the-Loop (CeTI) of Technische Universität Dresden. The authors would like to thank the Bavarian State Ministry for Economic Affairs, Regional Development and Energy (StMWi) for financial support as part of the project SafeRoBAY (grant number: DIK0203/01) and KI.FABRIK (Phase 1: Infrastructure and research and development program DIK0249). Please note that S. Haddadin has a potential conflict of interest as shareholder of Franka Emika GmbH.

REFERENCES

[1] ISO 9283:1998-04, Manipulating industrial robots - Performance criteria and related test methods (ISO 9283:1998).

[2] S. Wrede, C. Emmerich, R. Grünberg, A. Nordmann, A. Swadzba, and J. Steil, "A user study on kinesthetic teaching of redundant robots in task and configuration space," *Journal of Human-Robot Interaction Steering Committee*, vol. 2, no. 1, 2013.

[3] G. F. Rossano, C. Martinez, M. Hedelind, S. Murphy, and T. A. Fuhlbrigge, "Easy robot programming concepts: An industrial perspective," in *IEEE International Conference on Automation Science and Engineering (CASE)*, 2013, pp. 1119–1126.

[4] DIN ISO/TS 15066:2016-02, Robots and robotic devices - Collaborative robots (ISO/TS 15066:2016).

[5] K. Fischer, F. Kirstein, L. C. Jensen, N. Krüger, K. Kukliski, M. V. aus der Wieschen, and T. R. Savarimuthu, "A comparison of types of robot control for programming by demonstration," in *ACM/IEEE International Conference on Human-Robot Interaction*, 2016, pp. 213–220.

[6] T. Gašpar, M. Deniša, P. Radanovič, B. Ridge, T. R. Savarimuthu, A. Kramberger, M. Priggemeyer, J. Roßmann, F. Wörgötter, T. Ivanovska, S. Parizi, Ž. Gosar, I. Kovač, and A. Ude, "Smart hardware integration with advanced robot programming technologies for efficient reconfiguration of robot workcells," *Robotics and Computer-Integrated Manufacturing*, vol. 66, p. 101979, 2020.

[7] B. Akgun, M. Cakmak, and J. W. Y. nd A. L. Thomaz, "Trajectories and keyframes for kinesthetic teaching: A human-robot interaction perspective," in *ACM/IEEE International Conference on Human-Robot Interaction*. New York, NY, USA: Association for Computing Machinery, 2012.

[8] A. Albu-Schäffer, "Regelung von Robotern mit elastischen Gelenken am Beispiel der DLR-Leichtbauarme," Ph.D. dissertation, Technischen Universität München, 2002, (German).

[9] D. Lee and C. Ott, "Incremental kinesthetic teaching of motion primitives using the motion refinement tube," *Autonomous Robots*, vol. 31, no. 2, pp. 115–131, 2011.

[10] C. Ott, R. Mukherjee, and Y. Nakamura, "Unified impedance and admittance control," in *IEEE Int. Conf. on Robotics and Automation (ICRA)*, 2010, pp. 554–561.

[11] S. Tittel, M. Malekzadeh, and J. Steil, "Full 6-dof admittance control for the industrial robot stäubli tx60," in *IEEE International Conference on Automation Science and Engineering (CASE)*, 2019, pp. 1450–1455.

[12] R. J. Kirschner, A. Kurdas, K. Karacan, P. Junge, S. Birjandi, N. Mansfeld, S. Abdolshah, and S. Haddadin, "Towards a reference framework for tactile robot performance and safety benchmarking," in *2021 IEEE/RSJ International Conference on Intelligent Robots and Systems (IROS)*. IEEE, 2021, pp. 4290–4297.

[13] K. Fujikoshi, "Balancing apparatus for jointed robot," *Patent No. JP51*, vol. 122254, 1976.

[14] A. Bayer and G. Merk, "Industrial robot with a weight balancing system," *Patent EP*, vol. 2, no. 301, p. 727, 2011.

[15] V. Arakelian, "Gravity compensation in robotics," *Advanced Robotics*, vol. 30, no. 2, pp. 79–96, 2016.

[16] H.-S. Kim and J.-B. Song, "Multi-dof counterbalance mechanism for a service robot arm," *IEEE/ASME Transactions on Mechatronics*, vol. 19, no. 6, pp. 1756–1763, 2014.

[17] D. Lee and T. Seo, "Lightweight multi-dof manipulator with wire-driven gravity compensation mechanism," *IEEE/ASME Transactions on Mechatronics*, vol. 22, no. 3, pp. 1308–1314, 2017.

[18] M. Hanses, R. Behrens, and N. Elkmann, "Hand-guiding robots along predefined geometric paths under hard joint constraints," in *2016 IEEE 21st International Conference on Emerging Technologies and Factory Automation (ETFA)*, 2016, pp. 1–5.

[19] A. Winkler and J. Suchý, "Force-guided motions of a 6-d.o.f. industrial robot with a joint space approach," *Advanced Robotics*, vol. 20, no. 9, pp. 1067–1084, 2006.

[20] S. Lee, K. Ahn, and J. Song, "Torque control based sensorless hand guiding for direct robot teaching," in *IEEE/RSJ Int. Conf. on Intelligent Robots and Systems (IROS)*, 2016, pp. 745–750.

[21] R. Kikuuwe and H. Fujimoto, "Proxy-based sliding mode control for accurate and safe position control," in *IEEE Int. Conf. on Robotics and Automation (ICRA)*, 2006, pp. 25–30.

[22] M. Saveriano, S. An, and D. Lee, "Incremental kinesthetic teaching of end-effector and null-space motion primitives," in *IEEE Int. Conf. on Robotics and Automation (ICRA)*, 2015, pp. 3570–3575.

[23] M. Simonič, T. Petrič, A. Ude, and B. Nemec, "Analysis of methods for incremental policy refinement by kinesthetic guidance," *Journal of Intelligent & Robotic Systems*, vol. 102, no. 1, pp. 1–19, 2021.

[24] F. Lagriffoul, N. T. Dantam, C. Garrett, A. Akbari, S. Srivastava, and L. E. Kavraki, "Platform-independent benchmarks for task and motion planning," *IEEE Robotics and Automation Letters*, vol. 3, no. 4, pp. 3765–3772, 2018.

[25] A. Garg, D. B. Chaffin, and G. D. Herrin, "Prediction of metabolic rates for manual materials handling jobs," *American Industrial Hygiene Association Journal*, vol. 39, no. 8, pp. 661–674, 1978, pMID: 696629. [Online]. Available: https://doi.org/10.1080/0002889778507831

[26] B. Alkan, D. Vera, M. Ahmad, B. Ahmad, and R. Harrison, "A lightweight approach for human factor assessment in virtual assembly designs: An evaluation model for postural risk and metabolic workload," *Procedia CIRP*, vol. 44, pp. 26–31, 2016, 6th CIRP Conference on Assembly Technologies and Systems (CATS). [Online]. Available: https://www.sciencedirect.com/science/article/pii/S2212827116003978